A NONREDUNDANT NF–FF TRANSFORMATION WITH SPHERICAL SPIRAL SCANNING USING A FLEXIBLE AUT MODEL

F. D'Agostino [1], F. Ferrara [1], J.A. Fordham [2], C. Gennarelli [1],
R. Guerriero [1], C. Rizzo [3]

(1) D.I.I.I.E. - University of Salerno, via Ponte Don Melillo, 84084 Fisciano (SA), Italy.
(2) MI Technologies, 1125 Satellite Blvd, Suite 100 Suwanee, Georgia 30024-4629, USA
(3) MI Technologies (Europe), Chichester, West Sussex, UK.

ABSTRACT

In this work, a probe compensated near-field – far-field transformation technique with spherical spiral scanning suitable to deal with elongated antennas is developed by properly applying the unified theory of spiral scans for nonspherical antennas. A very flexible source modelling, formed by a cylinder ended in two half-spheres, is considered as surface enclosing the antenna under test. It is so possible to obtain a remarkable reduction of the number of data to be acquired, thus significantly reducing the required measurement time. Some numerical tests, assessing the accuracy of the technique and its stability with respect to random errors affecting the data, are reported.

Keywords: Near-field – far-field transformation techniques, Spherical spiral scanning, Nonredundant sampling representations of electromagnetic fields, Flexible source modelling.

1. Introduction

Nowadays, the reduction of the time needed to collect the near-field data is a very important issue for the antenna measurements community. In fact, such a time is very much greater than that required to perform the near-field – far-field (NF–FF) transformations. To this end, the use of the modulated scattering technique using arrays of scattering probes, which allows a very fast electronic scanning, has been proposed in [1]. However, antenna testing NF facilities based on such a technique are not very flexible. When using mechanical scans, the time reduction requirement can be accomplished, as suggested in [2], by employing continuous and synchronized movements of the positioning systems of the probe and antenna under test (AUT). Accordingly, NF–FF transformation techniques using innovative spiral scannings have been recently developed [3-6]. They are based on the theoretical results concerning the nonredundant sampling representations of electromagnetic (EM) fields [7] and on the optimal sampling interpolation (OSI) expansions of central type. Accordingly, the NF data needed by the corresponding NF–FF transformation can be reconstructed by interpolating the nonredundant ones acquired on the spiral. The required two-dimensional algorithm has been obtained [6]: a) by assuming the AUT enclosed in the smallest sphere able to contain it; b) by developing a nonredundant sampling representation of the voltage on the spiral; c) by choosing the spiral step equal to the sample spacing required to interpolate the data along a meridian curve.

Among the NF–FF transformation techniques with spiral scannings, that employing the spherical spiral one gives the full antenna pattern coverage, even though the data processing is considerably more burdensome than that needed by planar and cylindrical NF facilities [3, 4].

Unfortunately, when dealing with antennas having two dimensions very different from the third one, the spherical AUT modelling induces a redundancy, which gives rise to useless increase in the number of the NF data to be acquired. In order to overcome this drawback, two effective NF–FF transformation techniques with spherical spiral scanning tailored for these kinds of antennas have been developed in [8], by properly applying the unified theory of spiral scannings for nonspherical antennas [9]. In particular, a prolate ellipsoidal modelling of the AUT has been adopted when dealing with elongated antennas, whereas an oblate ellipsoid has been employed to model quasi-planar ones.

A very flexible modelling, wherein the surface enclosing the AUT is a rounded cylinder, i.e., a cylinder ended in two half-spheres, is proposed in this work in order to develop an efficient probe compensated NF–FF transformation technique with spherical spiral scanning for elongated antennas. Such a model is more effective from the data reduction viewpoint than the prolate ellipsoidal one, since it allows one to fit better the shape of a lot of actual antennas by properly setting its geometric parameters.

2. The rounded cylinder modelling

Let us consider an AUT and a nondirective probe scanning a spiral wrapping a sphere of radius d in the NF region and adopt the spherical coordinate system (r,ϑ,φ) for denoting an observation point P (Fig. 1). Since the voltage V measured by a nondirective probe has the same effective spatial bandwidth of the field, the theoretical results relevant to the nonredundant sampling representation of EM fields [7] can be applied to it. Accordingly, by assuming the AUT as enclosed in the smallest sphere able to contain it (spherical AUT modelling) and describing the spiral by means of a proper analytical parameterization $\underline{r} = \underline{r}(\xi)$, the probe "reduced voltage"

$$\tilde{V}(\xi) = V(\xi)\, \mathrm{e}^{\mathrm{j}\gamma(\xi)}, \tag{1}$$

$\gamma(\xi)$ being a phase function to be determined, can be closely approximated by a spatially bandlimited function. The corresponding bandlimitation error becomes negligible as the bandwidth exceeds a critical value W_ξ [7], so that it can be effectively controlled by choosing a bandwidth equal to $\chi' W_\xi$, $\chi'>1$ being an excess bandwidth factor.

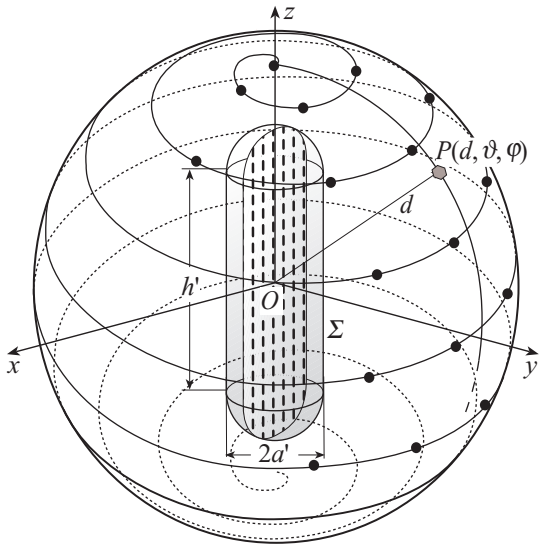

Figure 1 - Spherical spiral scanning.

When handling elongated antennas, it is no longer convenient to adopt the smallest sphere as surface enclosing them [6] but, as suggested in [9], a proper rotational surface Σ bounding a convex domain. A very flexible modelling can be obtained by considering the surface Σ formed by a cylinder of height h' ended in two half-spheres of radius a' (see Fig. 2). In such a way, it is possible to fit very well a lot of real antennas by properly choosing the values of h' and a'.

The unified theory of spiral scannings for nonspherical antennas [9], obtained by paralleling the corresponding rigorous procedure valid when adopting the spherical AUT modelling [6], allows one to develop the voltage sampling representation on the sphere from a nonredundant number of its samples collected on the spiral. To this end, it is necessary: a) to determine a nonredundant representation along the spiral; b) to choose the step of the spiral such that it intersects any meridian at points having the proper sample spacing needed for the interpolation. In particular, according to [9], the bandwidth W_η and parameterization η relevant to a meridian, and the corresponding phase function ψ are given by

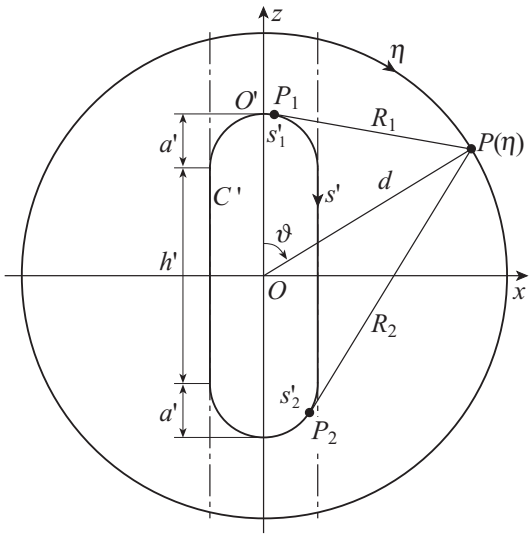

Figure 2 - Relevant to a meridian.

$$W_\eta = \beta \ell' / 2\pi \tag{2}$$

$$\eta = \frac{\pi}{\ell'}\left[R_1 - R_2 + s'_1 + s'_2\right] \tag{3}$$

$$\psi = \frac{\beta}{2}\left[R_1 + R_2 + s'_1 - s'_2\right] \tag{4}$$

where $\ell' = 2(h' + \pi a')$ is the length of the intersection curve between the meridian plane through P and Σ, $s'_{1,2}$ are the arclength coordinates of the two tangency points $P_{1,2}$, and $R_{1,2}$ the distances from P to $P_{1,2}$ (Fig. 2). The expressions of $R_{1,2}$ and $s'_{1,2}$ change depending on the location of $P_{1,2}$. In particular, three cases must be considered for ϑ ranging in $[0, \pi]$ (see Fig. 2). When $0 \le \vartheta \le \sin^{-1}(a'/d)$, it results:

$$R_1 = \sqrt{(d\sin\vartheta)^2 + (d\cos\vartheta - h'/2)^2 - a'^2} \tag{5}$$

$$s'_1 = a' \sin^{-1}\left(\frac{a' d\sin\vartheta + R_1(h'/2 - d\cos\vartheta)}{R_1^2 + a'^2}\right) \tag{6}$$

$$R_2 = R_1 \tag{7}$$

$$s'_2 = a' \sin^{-1}\left(\frac{a' d\sin\vartheta - R_2(h'/2 - d\cos\vartheta)}{R_2^2 + a'^2}\right) \tag{8}$$

When $\sin^{-1}(a'/d) \le \vartheta \le \pi - \sin^{-1}(a'/d)$, the expressions of R_1 and s_1' are again given by relations (5) and (6), whereas it results:

$$R_2 = \sqrt{(d\sin\vartheta)^2 + (d\cos\vartheta + h'/2)^2 - a'^2} \tag{9}$$

$$s_2' = h' + a'\left[\pi - \sin^{-1}\left(\frac{a'd\sin\vartheta + R_2(h'/2 + d\cos\vartheta)}{R_2^2 + a'^2}\right)\right] \tag{10}$$

When $\pi - \sin^{-1}(a'/d) \le \vartheta \le \pi$, the expressions of R_2 and s_2' are again given by relations (9) and (10), whereas it results:

$$R_1 = \sqrt{(d\sin\vartheta)^2 + (d\cos\vartheta + h'/2)^2 - a'^2} \tag{11}$$

$$s_1' = h' + a'\left[\frac{\pi}{2} - \sin^{-1}\left(\frac{R_1 d\sin\vartheta + a'(h'/2 + d\cos\vartheta)}{R_1^2 + a'^2}\right)\right] \tag{12}$$

According to [9], the spiral can be obtained by projecting on the scanning sphere a proper spiral wrapping the rounded cylinder. The spiral step is equal to the sample spacing $\Delta\eta = 2\pi/(2N''+1)$ needed to interpolate the voltage along a meridian. Note that $N'' = \mathrm{Int}(\chi N') + 1$, where $N' = \mathrm{Int}(\chi' W_\eta) + 1$ and $\chi > 1$ is an oversampling factor [7]. The projection is obtained via the curves at η = const (see Fig. 3). Accordingly, the equations of the spiral are:

$$\begin{cases} x = d\sin\theta(\eta)\cos\phi \\ y = d\sin\theta(\eta)\sin\phi \\ z = d\cos\theta(\eta) \end{cases} \tag{13}$$

wherein ϕ is the parameter describing the spiral and $\eta = k\phi = \phi/(2N''+1)$. It is worthy to note that the spiral angle θ, unlike the zenithal angle ϑ, can assume negative values.

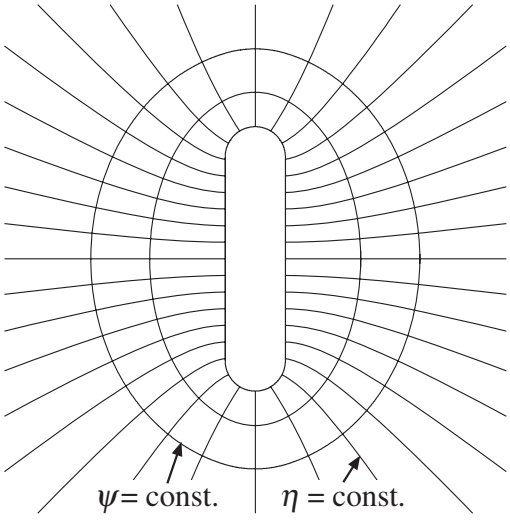

Figure 3 - Curves ψ = const and η = const.

The parameter ξ and phase factor γ to get a nonredundant representation along the spiral can be again determined by applying the unified theory [9]. In particular, γ coincides with the phase function ψ relevant to a meridian and ξ is β/W_ξ times the arclength of the projecting point that lies on the spiral wrapping Σ. Moreover, W_ξ is chosen equal to β/π times the length of the spiral wrapping the surface Σ from pole to pole.

In light of the above results, the reduced voltage at any point Q of the spiral can be recovered via the OSI expansion [9]:

$$\tilde{V}(\xi) = \sum_{m=m_0-p+1}^{m_0+p} \tilde{V}(\xi_m)\,\Omega_M(\xi - \xi_m)\,D_{M''}(\xi - \xi_m) \tag{14}$$

where $2p$ is the number of retained samples $\tilde{V}(\xi_m)$, $m_0 = \mathrm{Int}(\xi/\Delta\xi)$ the index of the sample nearest (on the left) to Q, and

$$\xi_m = m\Delta\xi = 2\pi m/(2M''+1) \tag{15}$$

with $M'' = \mathrm{Int}(\chi M') + 1$ and $M' = \mathrm{Int}(\chi' W_\xi) + 1$. Moreover,

$$D_{M''}(\xi) = \frac{\sin\left((2M''+1)\xi/2\right)}{(2M''+1)\sin(\xi/2)} \tag{16}$$

$$\Omega_M(\xi) = \frac{T_M\left[-1 + 2\left(\cos(\xi/2)/\cos(\bar{\xi}/2)\right)^2\right]}{T_M\left[-1 + 2/\cos^2(\bar{\xi}/2)\right]} \tag{17}$$

are the Dirichlet and Tschebyscheff Sampling functions, wherein $T_M(\xi)$ is the Tschebyscheff polynomial of degree $M = M'' - M'$ and $\bar{\xi} = p\Delta\xi$. It must be stressed that, when interpolating the voltage in the neighbourhood of the poles ($\vartheta = 0$ and $\vartheta = \pi$), it is necessary to increase the excess bandwidth factor χ' to avoid a significant growth of the bandlimitation error. This is mainly due to the fact that small variations of ξ correspond to very large changes of ϕ in these zones [6, 9]. The OSI formula (14) can be used to evaluate the "intermediate samples", namely, the reduced voltage values at the intersection points between the spiral and the meridian passing through P. Once these samples have been evaluated, the reduced voltage at P can be reconstructed via the following OSI expansion:

$$\tilde{V}(\eta(\vartheta), \varphi) = \sum_{n=n_0-q+1}^{n_0+q} \tilde{V}(\eta_n)\,\Omega_N(\eta - \eta_n)\,D_{N''}(\eta - \eta_n) \tag{18}$$

where $N = N'' - N'$, $n_0 = \mathrm{Int}[(\eta - \eta_0)/\Delta\eta)]$, $2q$ is the number of the retained intermediate samples $\tilde{V}(\eta_n)$,

$$\eta_n = \eta_n(\varphi) = k\varphi + n\Delta\eta = \eta_0 + n\Delta\eta \tag{19}$$

and the other symbols have the same or analogous meaning as in (14). It is so possible to get the NF data needed to perform the spherical NF–FF transformation [10], as modified in [11].

3. Numerical results

The following simulations refer to a spiral wrapping a sphere of radius $d = 35\lambda$ and to a uniform planar array of elementary Huygens sources polarized along the z axis, spaced by 0.5λ (λ being the wavelength). These sources cover a zone in the plane $y = 0$, formed by a rectangle ended in two half-circles. The sizes of the rectangle are: $2a' = 10\lambda$ and $h' = 36\lambda$. An open-ended circular waveguide, having radius $\rho' = 0.338\lambda$, is considered as measurement probe. Figures 4 and 5 show the reconstruction of the amplitude and phase of the rotated probe voltage V' on the meridian at $\varphi = 90°$. As can be seen, there is an excellent agreement between the exact voltage and the reconstructed one. It is useful to note that we have adopted, in the zones of the spiral determined by the 40 samples around the poles, an excess bandwidth factor such that the sample spacing is reduced exactly by a factor 7. The accuracy in the interpolation process is also confirmed by the values of the maximum and mean-square errors (normalized to the voltage maximum value on the sphere) reported in Figs. 6 and 7 for $p = q$ ranging from 3 to 10, $\chi' = 1.20$ (save for the polar zones), and $\chi = 1.10,\ 1.15,\ 1.20,\ 1.25$. As expected, they decrease up to very low values on increasing the oversampling factor and/or the number of retained samples. The algorithm robustness has been verified by adding random errors to the exact samples. These errors simulate a background noise (bounded to Δa in amplitude and with arbitrary phase) and an uncertainty on the samples of $\pm\Delta a_r$ in amplitude and $\pm\Delta\alpha$ in phase. As shown in Figs. 8 and 9, the algorithm works well also in presence of error affected data. The reconstructions of the antenna FF pattern in the principal planes are shown in Figs. 10 and 11. As can be seen, the reconstructions are very accurate.

It is useful to note that the number of samples on the spiral is 14 162, significantly less than that (57 550) required by the approach proposed in [6]. In particular, the number of "regular samples" at spacing $\Delta\xi$ is 13 202, whereas the number of "extra samples" at reduced spacing is 960. Moreover, the number of used samples results to be much less than that (130 562) needed by the classical NF–FF transformation with spherical scanning [10].

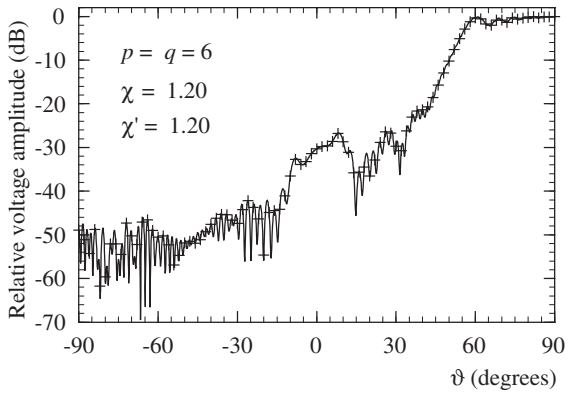

Figure 4 - Amplitude of V' on the meridian at $\varphi = 90°$. Solid line: exact. Crosses: interpolated.

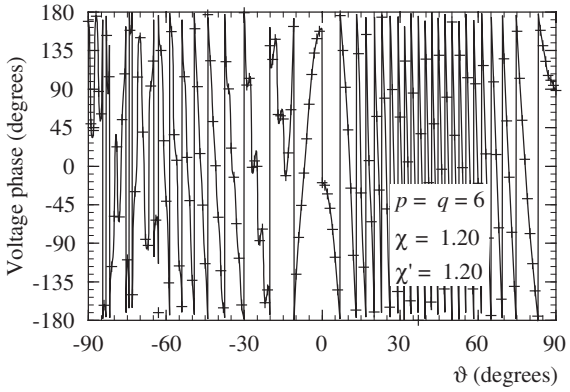

Figure 5 - Phase of V' on the meridian at $\varphi = 90°$. Solid line: exact. Crosses: interpolated.

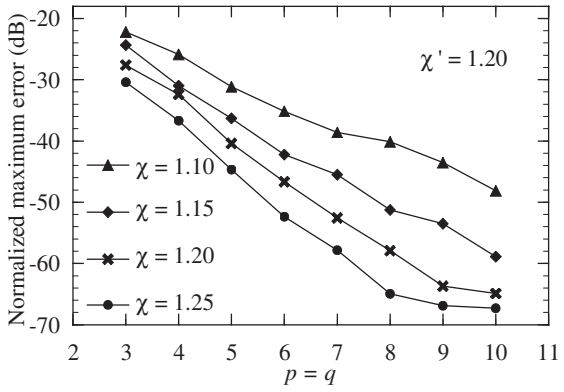

Figure 6 - Normalized maximum errors in the reconstruction of V'.

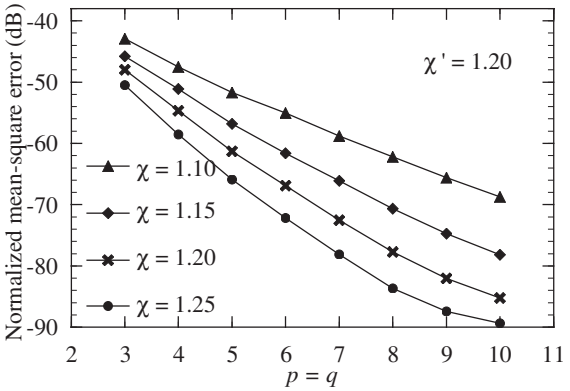

Figure 7 - Normalized mean-square errors in the reconstruction of V'.

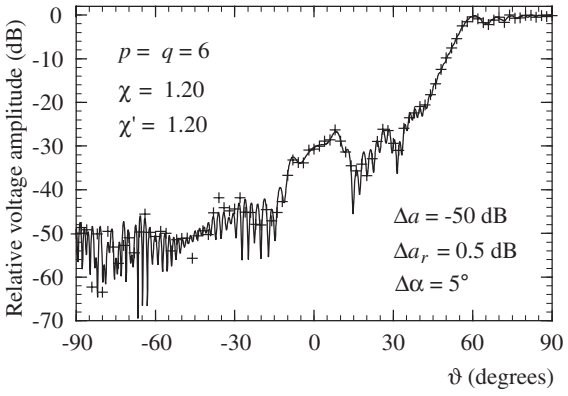

Figure 8 - Amplitude of V' on the meridian at $\varphi = 90°$. Solid line: exact. Crosses: interpolated from error affected data.

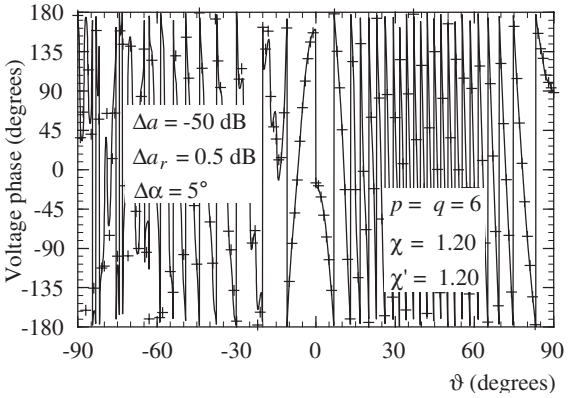

Figure 9 - Phase of V' on the meridian at $\varphi = 90°$. Solid line: exact. Crosses: interpolated from error affected data.

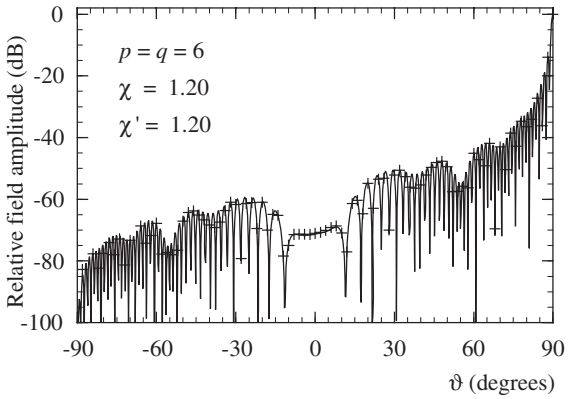

Figure 10 - E-plane pattern. Solid line: exact. Crosses: reconstructed from NF measurements.

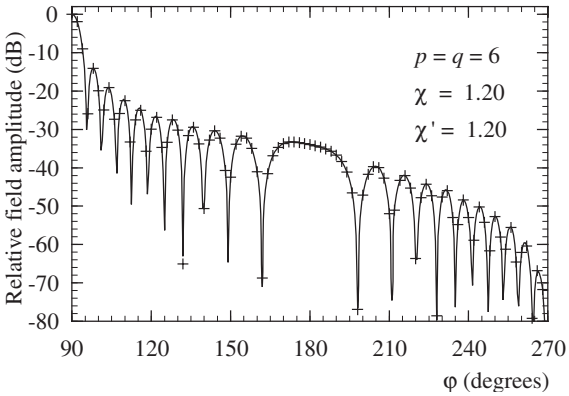

Figure 11 - H-plane pattern. Solid line: exact. Crosses: reconstructed from NF measurements.

4. REFERENCES

[1] J.C.Bolomey et alii, "Rapid near-field antenna testing via array of modulated scattering probes," *IEEE Trans. Antennas Prop.*, vol. AP-36, pp. 804–814, 1988.

[2] R.G.Yaccarino, L.I.Williams, and Y.Rahmat-Samii, "Linear spiral sampling for the bipolar planar antenna measurement technique," *IEEE Trans. Antennas Prop.*, vol. AP-44, pp. 1049-1051, 1996.

[3] O.M.Bucci, C.Gennarelli, G.Riccio, and C.Savarese, "Nonredundant NF–FF transformation with helicoidal scanning," *J. Electrom. Waves Appl.,* vol. 15, pp. 1507-1519, 2001.

[4] O.M.Bucci, F.D'Agostino, C.Gennarelli, G.Riccio, and C.Savarese, "Probe compensated FF reconstruction by NF planar spiral scanning," *IEE Proc. - Microw., Antennas Prop.,* vol. 149, pp. 119-123, 2002.

[5] O.M.Bucci, F.D'Agostino, C.Gennarelli, G.Riccio, and C.Savarese, "NF–FF transformation with spherical spiral scanning," *IEEE Antennas Wireless Prop. Lett.*, vol. 2, pp. 263-266, 2003.

[6] F.D'Agostino, C.Gennarelli, G.Riccio, and C.Savarese, "Theoretical foundations of near-field–far-field transformations with spiral scannings," *Prog. in Electrom. Res.*, vol. PIER 61, pp. 193-214, 2006.

[7] O.M.Bucci, C.Gennarelli, and C.Savarese, "Representation of electromagnetic fields over arbitrary surfaces by a finite and nonredundant number of samples," *IEEE Trans. Antennas Prop.*, vol. 46, pp. 351-359, 1998.

[8] F.D'Agostino, F.Ferrara, C.Gennarelli, R.Guerriero, M.Migliozzi, and G.Riccio, "A nonredundant near-field to far-field transformation with spherical spiral scanning for nonspherical antennas," *The Open Elect. & Electronic Eng. J.*, vol. 3, pp. 4-11, 2009.

[9] F.D'Agostino, F.Ferrara, C.Gennarelli, R.Guerriero, and M.Migliozzi, "The unified theory of near–field – far–field transformations with spiral scannings for nonspherical antennas," *Prog. in Electrom. Res. B*, vol. 14, pp. 449-477, 2009.

[10] J.E.Hansen, *Spherical near-field antenna measurements*, IEE Electromagnetic Waves Series, London, Peter Peregrinus Ltd., UK, 1998.

[11] O.M.Bucci, F.D'Agostino, C.Gennarelli, G.Riccio, and C.Savarese, "Data reduction in the NF–FF transformation technique with spherical scanning," *J. Electrom. Waves Appl.,* vol. 15, pp. 755-775, 2001.